Electronic Supporting Information

An excellent multifunctional photocatalyst cooperated by polyoxometalate-viologen framework for CEES oxidation, Cr(VI) reduction and dyes decolorization under different light regimes

Lin Yang, Zhong Zhang,* Chaonan Zhang, Shuang Li, Guocheng Liu and Xiuli Wang*

College of Chemistry and Materials Engineering, Professional Technology Innovation Center of Liaoning Province for Conversion Materials of Solar Cell, Bohai University, Jinzhou 121013, China. E-mail: zhangzhong666@126.com (Zhong Zhang), wangxiuli@bhu.edu.cn (Xiuli Wang)

Table S1 Crystallographic data for **BHU-1**

Empirical formula	$C_{36}H_{38}CoMo_4N_4O_{22}$
Formula weight	1321.39
Crystal system	triclinic
Space group	*P*-1
a (Å)	12.6447(13)
b (Å)	13.9655(13)
c (Å)	14.9485(14)
α (°)	63.048(2)
β (°)	67.079(2)
γ (°)	69.823(2)
V (Å^3)	2121.2(4)
Z	2
D_c (g/cm^3)	1.984
M (mm^{-1})	1.616
F(000)	1246.0
Reflections collected	12226
Unique reflections	7502
R_{int}	0.0364
GOF	0.971
R_1[a][I>=2σ(I)]	0.0424
wR_2[b] (all data)	0.0989

[a] $R_1=\sum||F_o|-|F_c||/\sum|F_o|$; [b] $wR_2=\Sigma[w(F_o^2-F_c^2)^2]/\Sigma[w(F_o^2)^2]^{1/2}$

Table S2 Bond lengths [Å] and angles [°] for **BHU-1**

Co(1)-O(4)#2	2.024(4)	O(1)-Co(1)-N(1)#3	94.83(17)
Co(1)-O(1)	2.100(4)	O(1)-Co(1)-N(3)#4	88.90(18)
Co(1)-O(3)	1.993(4)	O(3)-Co(1)-O(4)#2	122.61(17)
Co(1)-O(2)	2.363(4)	O(3)-Co(1)-O(1)	89.74(17)
Co(1)-N(1)#3	2.164(5)	O(3)-Co(1)-O(2)	146.56(17)
Co(1)-N(3)#4	2.203(5)	O(3)-Co(1)-N(1)#3	92.97(17)
O(4)#2-Co(1)-O(1)	146.74(16)	O(3)-Co(1)-N(3)#4	88.01(17)
O(4)#2-Co(1)-O(2)	88.58(16)	N(1)#3-Co(1)-O(2)	98.50(16)
O(4)#2-Co(1)-N(1)#3	91.25(17)	N(1)#3-Co(1)-N(3)#4	176.15(19)
O(4)#2-Co(1)-N(3)#4	85.09(17)	N(3)#4-Co(1)-O(2)	82.64(16)
O(1)-Co(1)-O(2)	58.18(15)		
Symmetry code for **BHU-1**: $^{\#2}$-X,2-Y,1-Z; $^{\#3}$-1+X,+Y,1+Z; $^{\#4}$+X,+Y,-1+Z			

Table S3 Bond Valence Sum (BVS) calculations of all Mo, Ni and selected O atoms in **BHU-1**

	1-BVS		
Mo1	5.96	O1	1.78
Mo2	6.03	O2	1.64
Mo3	6.02	O3	1.86
Mo4	5.85	O4	1.86
Co1	1.82		

Table S4 The reported complexes based on POMs and viologen ligands

Compound	Dimension	Ref
$Co_2(bpdo)_4(H_2O)_6](\alpha\text{-}GeW_{12}O_{40})\}\cdot 4H_2O$	1D	[1]
$[Co_5(bpdo)_5(H_2O)_{18}][Co_4(H_2O)_2(B\text{-}\alpha\text{-}PW_9O_{34})_2]\cdot bpdo\cdot 10H_2O$	2D	
$[Cu_2(CPBPY)_4(H_2O)_2][PW_{12}O_{40}][OH]\cdot 6H_2O$	2D	[2]
$[Cu_2(H_2O)_3(CPBPY)_2(CuHPW_{11}O_{39})]\cdot 7H_2O$	1D	[3]
$(Bpyen)_2(Mo_8O_{26})]\cdot 2H_2O$	0D	[4]
$[(Pbpy)_2(Mo_8O_{26})]\cdot 4H_2O$		
$[Ag^{I}(bmypd)_{0.5}(\beta\text{-}Mo_8O_{26})_{0.5}]$	2D	[5]
$[Ag^{I}_2(bypy)_4(HSiW_{12}O_{40})_2]\cdot 14H_2O$	0D	
$[Ag^{I}(bypy)(\gamma\text{-}Mo_8O_{26})_{0.5}]$	2D	
$[Cu(PBPY)_2[SiW_{12}O_{40}]$	1D	[6]
$(Me_2NH_2)_3[PW_{11}ZnO_{40}]$	0D	[7]
$[\delta\text{-}Mo_8O_{26}](L)_2\cdot 2H_2O$	0D	[8]
$[(AV^{2+})(p\text{-}AV)(EuW_{10}O_{36})]_n\cdot 2nH_2O$	1D	[9]
$(AV^{2+})[H_2W_{12}O_{40}]\cdot 5H_2O$	0D	

$(C_{14}H_{11}N_{4O})_2[Mo_8O_{26}]$	0D	[10]
$\{[Co_2(bpdo)_4(H_2O)_6](\alpha\text{-}GeW_{12}O_{40})\}\bullet 4(H_2O)\}_n$	1D	[11]

Table S5 Conversion and selectivity of the oxidation of CEES to CEESO in every 1 min and under different solvents

Entry	H_2O_2 (mmol)	Catal. (μmol)	Solvent	Light	Time (min)	Conv. (%)	Sele. (%)
1	0.5	4	C_2H_5OH	Visible	5	98	97
2	0.5	4	CH_3CN	Visible	5	10	67
3	0.5	4	CH_2Cl_2	Visible	5	9	14
4	0.5	4	C_2H_5OH	Visible	1	38	86
5	0.5	4	C_2H_5OH	Visible	2	67	92
6	0.5	4	C_2H_5OH	Visible	3	84	94
7	0.5	4	C_2H_5OH	Visible	4	92	95
8	0.5	4	C_2H_5OH	Visible	5	98	97

Table S6 The concentration of Co ions in the solution after the photocatalytic reaction

Cycles	Co ions concentration (ppm)
1	0.223
2	0.275
3	0.237

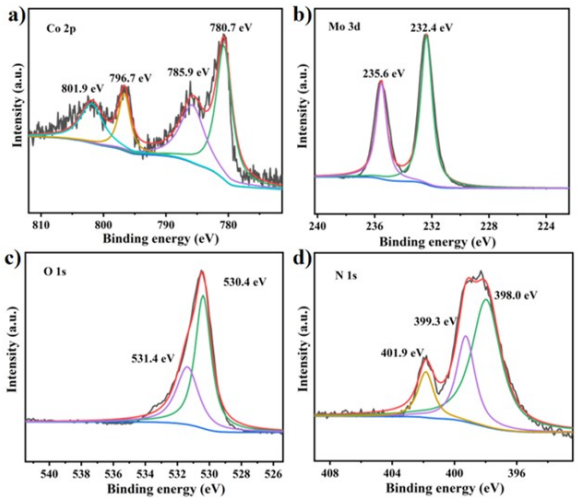

Fig. S1 The XPS spectra of **1**: a) Co 2p, b) Mo 3d, c) O 1s and d) N 1s.

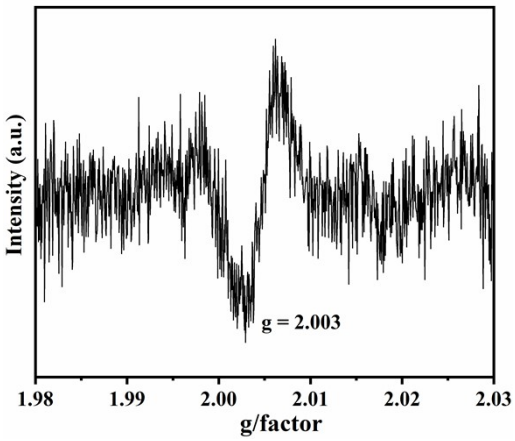

Fig. S2 The EPR spectrum of **BHU-1**.

The high resolution XPS spectra for Co 2p appear at 780.7 and 796.7 eV corresponding to Co $2p_{3/2}$ and Co $2p_{1/2}$ and obvious shake-up satellite features for Co $2p_{3/2}$ and Co $2p_{1/2}$ were also observed at 785.9 and 801.9 eV, respectively [12, 13]. The peaks of Mo 3d at 235.6 eV and 232.4 eV are assigned to Mo $3d_{5/2}$ and $3d_{3/2}$ orbitals of Mo^{6+} [14]. The O 1s state always contains low binding energy peak (LP) and high binding energy peak (HP) centred nearly at 530.4 and 531.4 eV [15]. The XPS N 1s spectra can be divided into 398.0 eV, 399.3 eV, which may be related to the N of pyridine and quaternary ammonium salt, the extra small peak at 401.9 eV corresponds to the nitrogen atom of the pyridyl radical with the EPR spectrum has a typical weak signal for the bipyridinium radical [16-19].

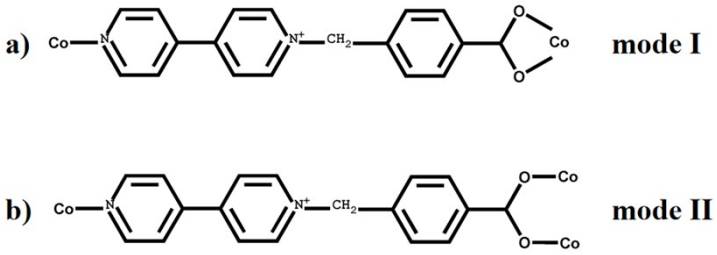

Fig. S3 Two types of coordination modes of bcbpy ligand: a) mode I, b) mode II.

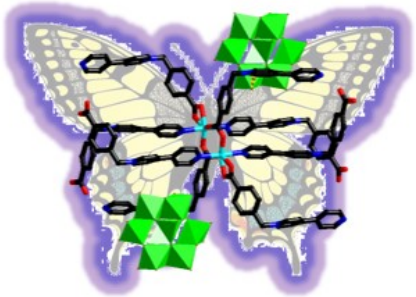

Fig. S4 The hydrogen-bond [C5-H5···O11: 2.982(10) Å] interaction between $[\theta\text{-}Mo_8O_{26}]^{4-}$ clusters and $[Co_2(bcbpy)_8]^{4+}$.

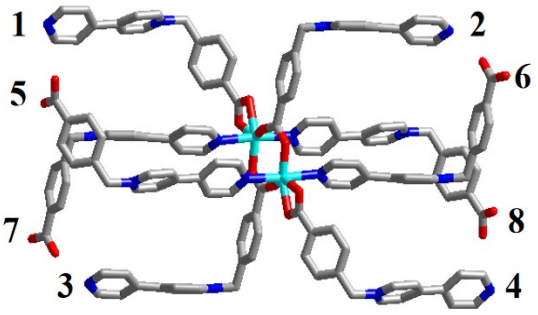

Fig. S5 Branches 1-8 in $[Co_2(bcbpy)_8]^{4+}$.

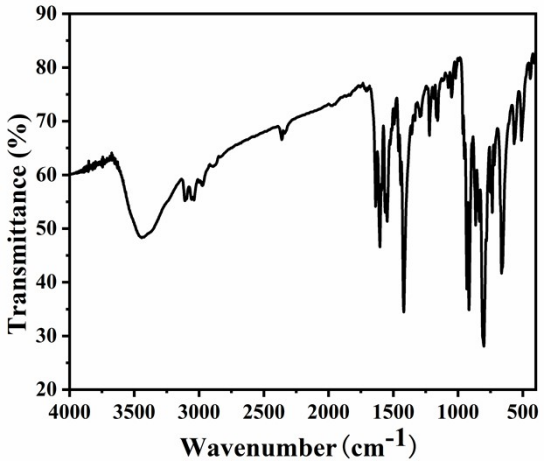

Fig. S6 IR spectrum of **BHU-1**.

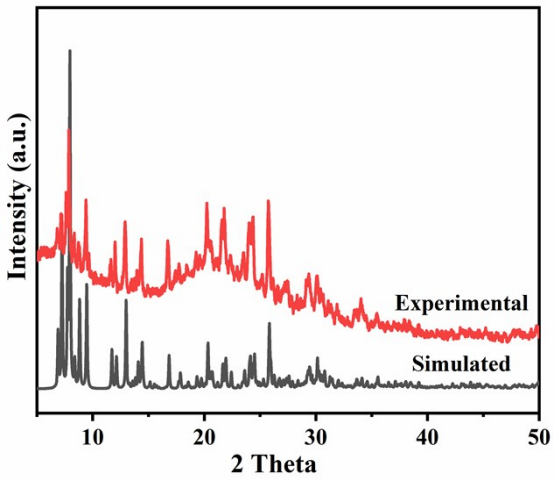

Fig. S7 Comparison of the experimental and simulated PXRD patterns of **BHU-1**.

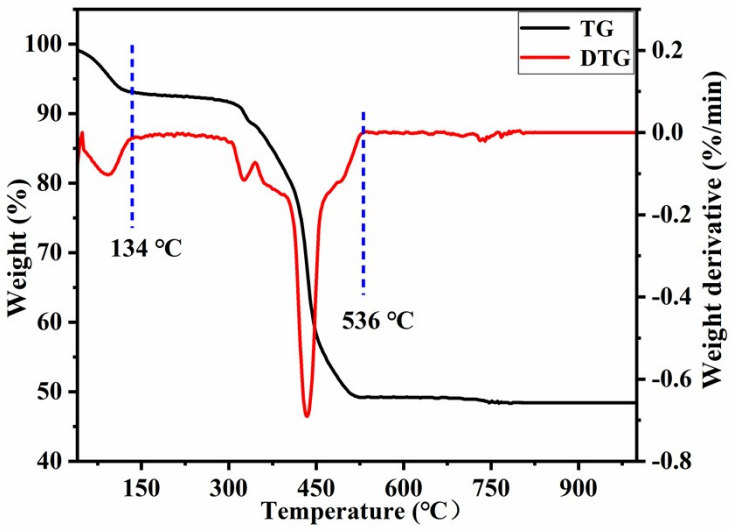

Fig. S8 TG and DTG curves of **BHU-1**.

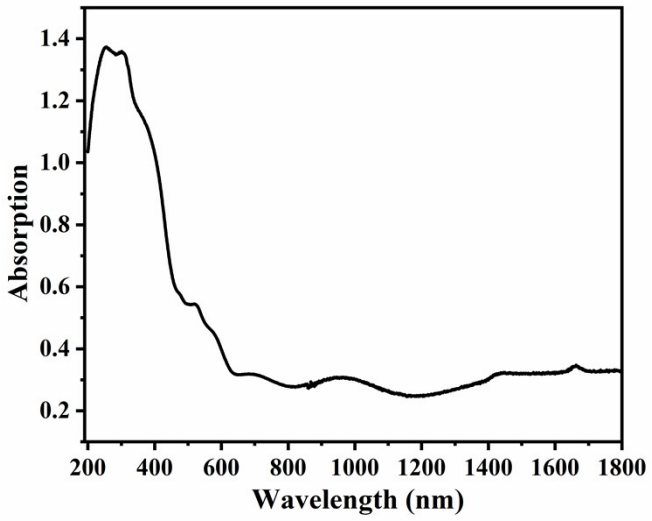

Fig. S9 UV-Vis-NIR absorption spectrum of **BHU-1**.

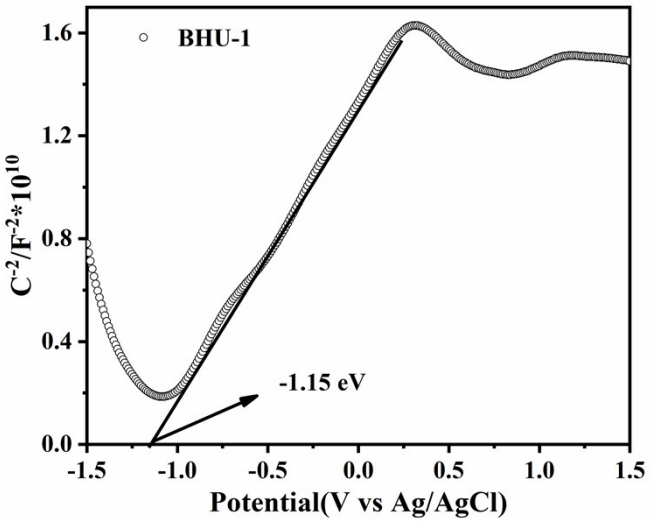

Fig. S10 Mott-Schottky plot of **BHU-1**.

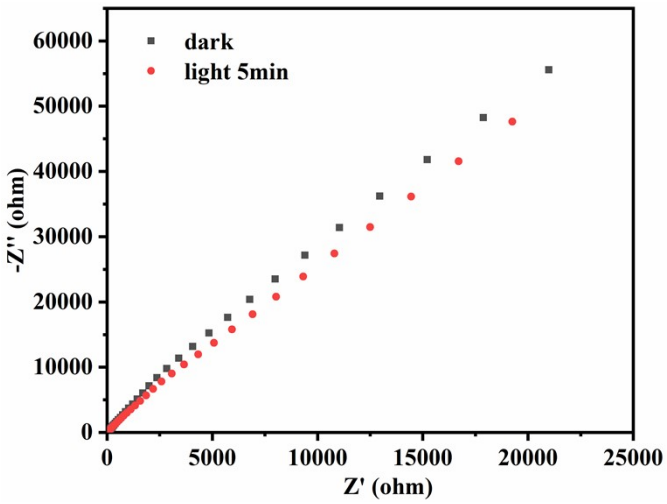

Fig. S11 EIS Nyquist plots of the **BHU-1** in 0.5 mol/L Na_2SO_4 solution under visible light irradiation.

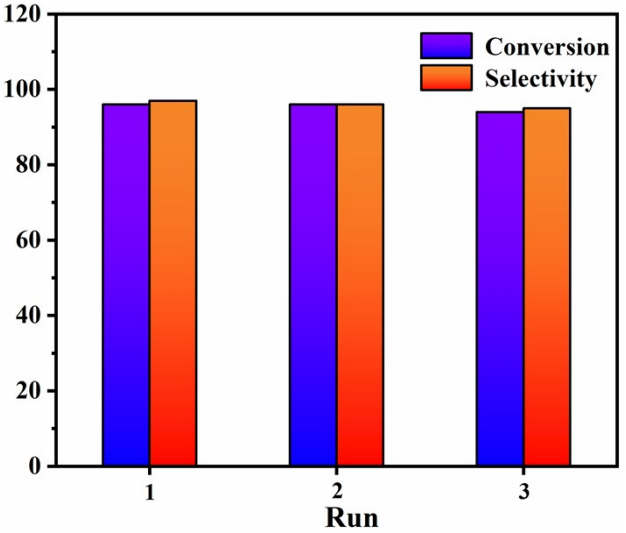

Fig. S12 The conversion and selectivity of CEES to CEESO after 3 cycles.

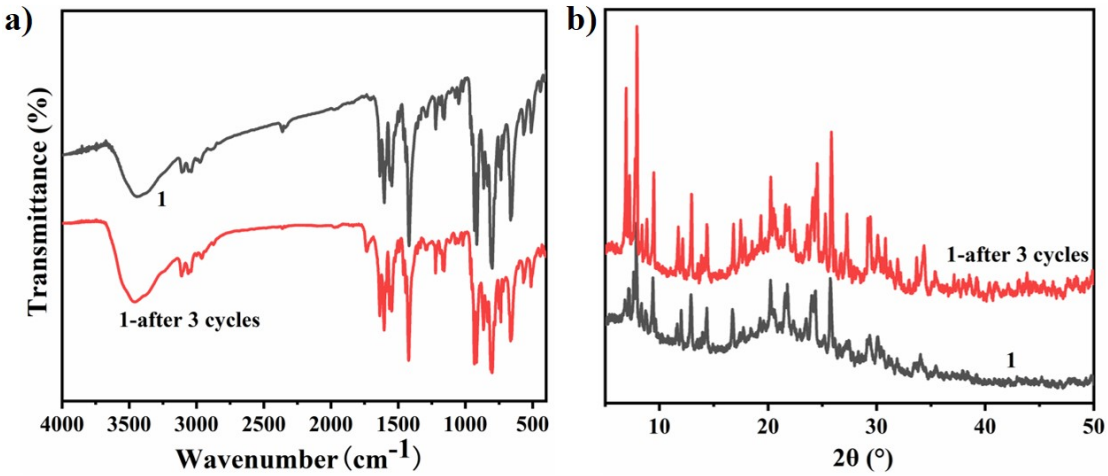

Fig. S13 The a) IR and b) PXRD spectra of **BHU-1** before and after 3 cycles for the oxidation of CEES.

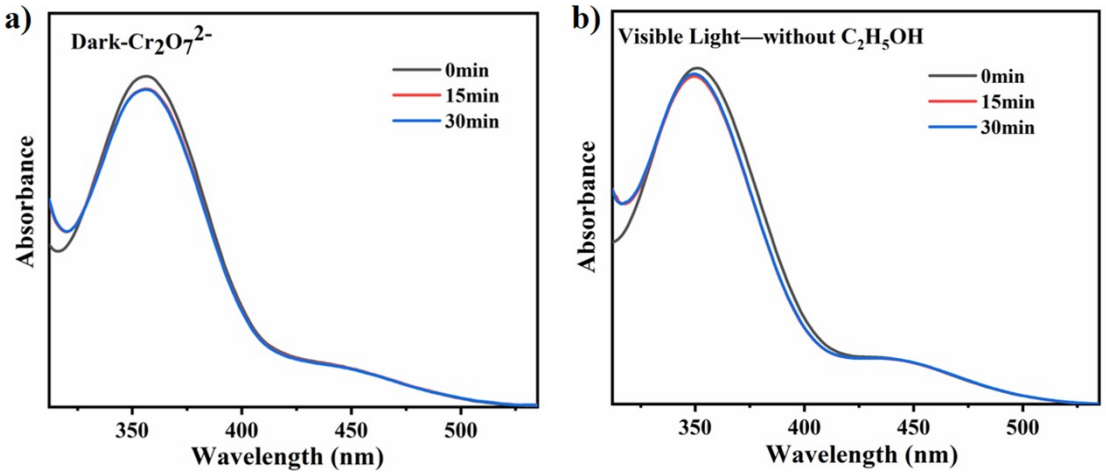

Fig. S14 Absorption spectra of the reduction of $Cr_2O_7^{2-}$ a) in the dark and b) without C_2H_5OH.

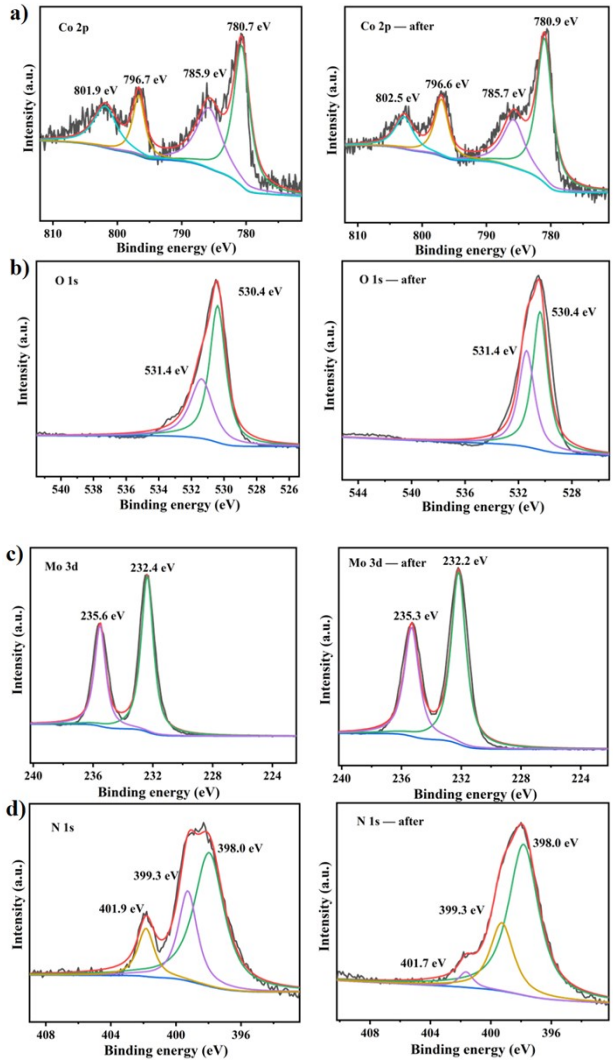

Fig. S15 The a) Co, b) O, c) Mo, d) N XPS spectra of **BHU-1** before and after photoreduction.

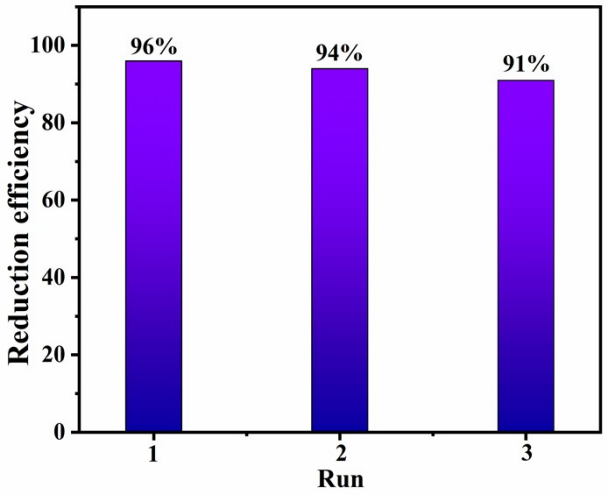

Fig. S16 The decolorization rate of RhB under visible light irradiation after 3 cycles.

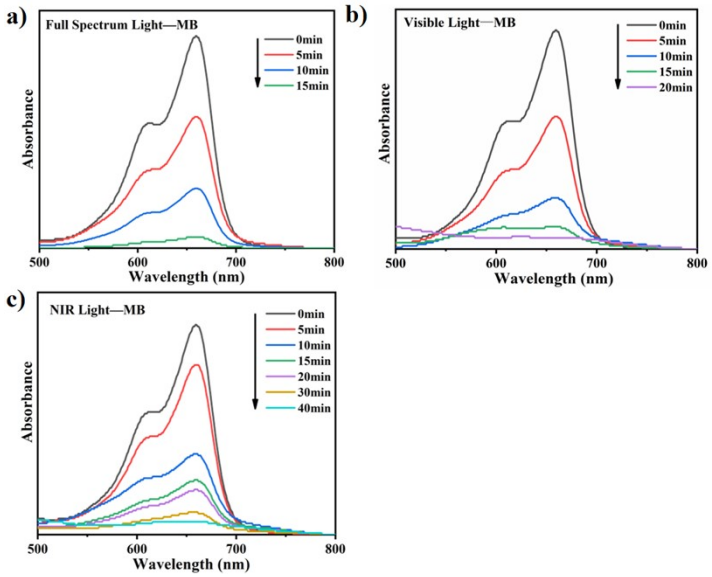

Fig. S17 a-c) Absorption spectra of the MB solution in the presence of **BHU-1** under full spectrum, visible, and NIR light irradiation, respectively.

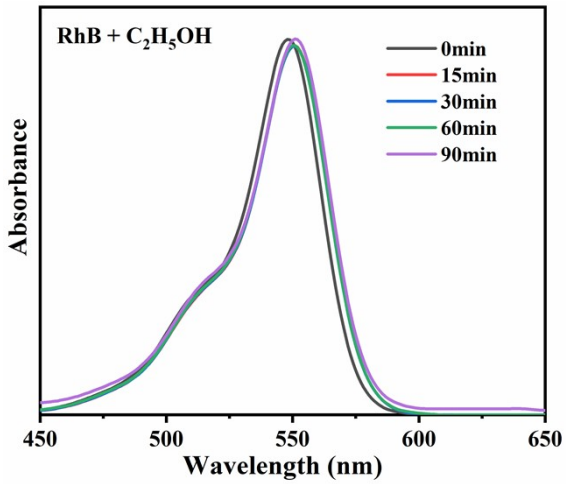

Fig. S18 Absorption spectra of the RhB solution in the presence of C_2H_5OH under the visible light irradiation.

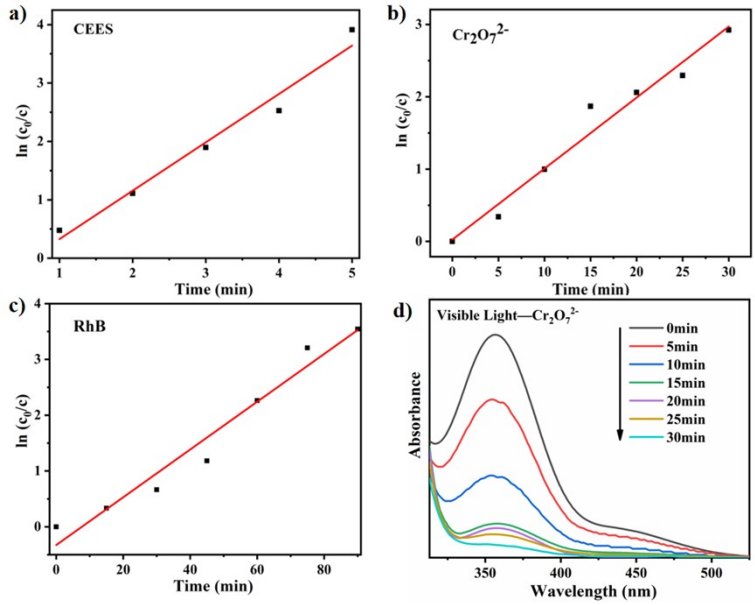

Fig. S19 a-c) The linear plot of ln(c_0/c) vs. reaction time (t) of CEES, Cr(VI) and RhB. d) Absorption spectra of the reduction of $Cr_2O_7^{2-}$ under visible light irradiation every 5 min.

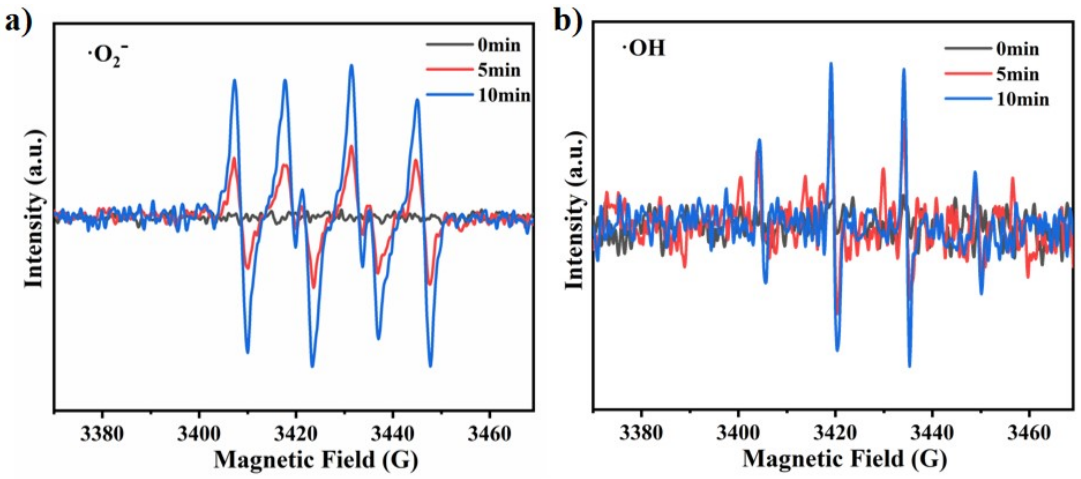

Fig. S20 EPR spectra of DMPO-adducts: a) $\cdot O_2^-$ and b) ·OH for **BHU-1**.

References

[1] Y. R. Huang, X. L. Lin, B. Chen, H. D. Zheng, Z. R. Chen, H. H. Li and S. T. Zheng, Thermal-responsive polyoxometalate-metalloviologen hybrid: reversible intermolecular three-Component reaction and temperature-regulated resistive switching behaviors*, Angew. Chem. Int. Ed.*, 2021, **60**, 16911-16916.

[2] X. J. Sun, J. Zhang and Z. Y. Fu, Polyoxometalate cluster sensitized with copper-viologen framework for efficient degradation of organic dye in ultraviolet, visible, and near-infrared light*, ACS Appl. Mater. Interfaces*, 2018, **10**, 35671-35675.

[3] X. J. Sun, J. Zhang, A. D. Tan and Z. Y. Fu, A highly efficient near-infrared-activated photocatalyst based on an electron-deficient copper-viologen-polyoxometalate framework with a copper {Cu3} cluster decorated phosphotungstate as a building block, *Cryst. Grow. Des.*, 2019,

19, 6845-6849.

[4] L. Li, J. R. Wang, Y. Hua, Y. Guo, C. Fu, Y. N. Sun and H. Zhang, ‘‘Reversible’’ photochromism of polyoxomolybdate–viologen hybrids without the need for proton transfer, *J. Mater. Chem. C*, 2019, **7**, 38-42.

[5] J. Ying, L. Jin, C. X. Sun, A. X. Tian and X. L. Wang, A series of polyoxometalate-viologen photochromic materials for UV probing, amine detecting and inkless and erasable printing, *Chem. Eur. J.*, 2022, **28**, e202103268.

[6] X. J. Sun, J. Zhang, X. Z. Yuan and Z. Y. Fu, A silicotungstate-based copper–viologen hybrid photocatalytic compound for efficient degradation of organic dyes under visible light, *CrystEngComm*, 2019, **21**, 5563-5567.

[7] L. Li, Y. C. Zou, Y. Hua, X. N. Li, Z. H. Wang and H. Zhang, Polyoxometalate-viologen photochromic hybrids for rapid solar ultraviolet light detection, photoluminescence-based UV probing and inkless and erasable printing, *Dalton Trans*, 2020, **49**, 89-94.

[8] X. X. Song, H. F. Fu, P. Wang, H. Y. Li, Y. Q. Zhang and C. C. Wang, The selectively fluorescent sensing detection and adsorptive removal of Pb^{2+} with a stable [δ-Mo_8O_{26}]-based hybrid, *J. Colloid Interface Sci.*, 2018, **532**, 598-604.

[9] D. F. Shen, S. Li, H. Liu, W. Jiang, Q. Zhang and G. G. Gao, A durable and fast-responsive photochromic and switchable luminescent polyviologen–polyoxometalate hybrid, *J. Mater. Chem. C*, 2015, **3,** 12090-12097.

[10] L. Li, Y. Hua, Y. Guo, G. S. Zhang, X. N. Li and H. Zhang, Viologen as a colour modulator in photochromism of polyoxomolybdate–viologen hybrids, *Eur. J. Inorg. Chem.*, 2018, **33**, 3757-3760.

[11] B. Chen, Y. R. Huang, K. Y. Song, X. L. Lin, H. H. Li and Z. R. Chen, Molecular nonvolatile memory based on [α-$GeW_{12}O_{40}$]$^{4-}$/metalloviologen hybrids can work at high temperature monitored by chromism, *Chem. Mater.*, 2021, **33**, 2178-2186.

[12] E. B. Castro, C. A. Gervasi, Electrodeposited Ni-Co-oxide electrodes: characterization and kinetics of the oxygen evolution reaction, *Int. J. Hydrogen Energy*, 2000, **25**, 1163-1170.

[13] H. M. Liu, G. L. Wei, Z. Xu, P. Liu and Y. Li, Quantitative analysis of Fe and Co in Co-substituted magnetite using XPS: The application of non-linear least squares fitting (NLLSF), *Appl. Surf. Sci.*, 2016, **389**, 438-446.

[14] X. X. Song, H. F. Fu, P. Wang, H. Y. Li, Y. Q. Zhang and C. C. Wang, The selectively fluorescent sensing detection and adsorptive removal of Pb^{2+} with a stable [δ-Mo_8O_{26}]-based hybrid, *J. Colloid Interface Sci.*, 2018, **532**, 598–604.

[15] R. Li, L. y. Liu, B. M. Ming, Y. H. Ji and R. Z. Wang, Oxygen vacancy effect on photoluminescence of KNb_3O_8 nanosheets, *Appl. Surf. Sci.*, 2018, **439**, 983-990.

[16] Z. Ren, Y. Liu, Y. Lyu, X. G. Song, C. Y. Zheng, S. Q. Feng, Z. Jiang and Y. J. Ding, Single-atom Rh based bipyridine framework porous organic polymer: A high active and superb stable catalyst for heterogeneous methanol carbonylation, *J. Catal.*, 2019, **369**, 249-256.

[17] J. Y. Jung, Y. L. Hong, J. G. Kim, M. J. Kim, Y. K. Kim and N. D. Kim, New insight of tailor-made graphene oxide for the formation of atomic Co-N sites toward hydrogen evolution reaction, *Appl. Surf. Sci.,* 2021, **563**, 150254.

[18] Y. X. Cui, L. Y. Yin, X. Y. Sun, N. Zhang, N. Gao and G. S. Zhu, A universal and reversible wet adhesive via straightforward aqueous self-assembly of polyethylenimine and polyoxometalate, *ACS Appl. Mater. Interfaces,* 2021, **13**, 47155–47162.

[19] X. D. Yang, L. Sun, C. Chen, Y. J. Zhang and J. Zhang, Anion-controlled photochromism of two bipyridinium-based coordination polymers and nondestructive luminescence readout, *Dalton Trans.*, 2017, **46**, 4366-4372.